Sensors and Materials, Vol. 10, No. 3 (1998) 139–154
MYU Tokyo

S & M 0320

Synthesis of SnO_{2-x} Thin Films by Oxygen-Ion-Assisted Deposition for Hydrocarbon Gas Detection

Dongsoo Choi, Seok-Kyun Song[1], Jin-Seok Jeon, Won-Kook Choi[1], Seok-Keun Koh[1], Ki-Dong Kim, Hyung-Jin Jung[1] and Hong-Koo Baik[2]

Division of Gas Utilization, R & D Center, Korea Gas Corporation,
Il-Dong 277-1, Ansan, Kyunggi-Do, Korea 425-150
[1]Ceramics Division, Korea Institute of Science and Technology,
Cheongryang, P.O. Box 131, Seoul, Korea 130-650
[2]Department of Metallurgical Engineering, Yonsei University,
Shincheon-Dong 134, Sudaemoon-Ku, Seoul, Korea 120-749

(Received January 27, 1997; accepted January 27, 1998)

Key words: tin oxide thin film, oxygen-ion-assisted deposition, hydrocarbon gas detection, substrates (SiO_2/Si, alumina), electrode position, dopants (Pt, Pd), ion beam energy

With the aim of developing efficient microsensors with low power consumption for the detection of inflammable hydrocarbon gases (CH_4, C_3H_8), SnO_2 thin films were synthesized and their gas sensing properties tested. Using an oxygen-ion-assisted deposition technique, a series of SnO_2 thin films with various crystalline structures and nonstoichiometry were prepared as a function of oxygen ion energy. The material properties of the synthesized thin films were investigated using X-ray diffraction (XRD), X-ray photoelectron spectroscopy (XPS), and transmission electron microscopy (TEM) and the sensing properties were determined based on the measurements of electrical conductance in a test gas environment.

The as-deposited tin oxide thin films were observed in an amorphous state and the annealed films showed a preferred orientation to the <110> axis, along with <101> and <211>. All the deposited films showed a deficiency in oxygen content as the state of SnO_{2-x} but had a binding energy of Sn^{+4}. With regard to differentiation in the sensitivities and selectivities of methane and propane, the effective factors were determined to be substrates (SiO_2/Si, alumina), electrode position, amount of dopants (Pt, Pd) and ion beam energy.

1. Introduction

Miniaturized gas sensors based on thin or thick films which consume very low power can be effectively used with regard to the sensitive and early detection of inflammable gas (CH_4 and C_3H_8) leakage from various industrial and residential gas-related equipment. Among several types of gas sensors, semiconducting oxides such as SnO_2, ZnO and Fe_2O_3 have been used extensively since reports of their gas sensing properties resulting from the change of surface conductance in the gaseous environment.[1,2] In particular, SnO_2 is the most versatile material in gas sensing elements in thick/thin films as well as bulk form.[3–6] However, it is still necessary to improve the gas-sensing properties of SnO_2 materials, especially for the case of thin/thick films, and to gain increased understanding of the working mechanisms and to obtain long-term stability.

It is well known that, in the case of thin/thick film applications, factors affecting the sensing properties of SnO_2 elements are the microstructure, stoichiometry, thickness, catalytic activity (dopants), operating temperature, substrate, and electrode position. In terms of optimizing gas-sensing properties, controlling these factors has been performed. To do this, ion beam techniques, which allow the design of material properties such as structure and stoichiometry, were considered to be the methods of choice. Using an oxygen-ion-assisted deposition (IAD) technique, this study was conducted mainly to improve and optimize the gas-sensing properties of SnO_2 thin film sensor elements with various material properties. To this end, a series of SnO_2 thin films with various crystalline structures and nonstoichiometry were prepared as a function of the oxygen ion energy and their gas sensing properties were tested in terms of dopants, electrode position and test temperature.

2. Materials and Methods

2.1 *Synthesis of tin oxide thin films for gas detection*

In order to grow tin oxide thin films, Si(100) wafers with an amorphous SiO_2 layer of 0.3 μm thickness and poly-Al_2O_3 plates were used as substrates. The film deposition process included the evaporation of Sn metal on the SiO_2/Si and the Al_2O_3 substrates as well as a 5 cm gridded cold hollow-cathode-type gas ion gun for the IAD of oxygen.

In the evaporation of the Sn metal, a molybdenum crucible with a cylindrical nozzle (1.5 mm(ϕ) × 1 mm) was used, and a pure Sn metal rod (99.995 +%, Aldrich Co.) was used as a source material. The temperature of the Mo crucible was slowly increased by resistive heating until the deposition rate of the Sn metal reached 0.3 Å/s without ionization potential (the so-called neutral metal beam (N-MB)). However, a small amount of ion current density ($J_{N\text{-}MB}$) was detected as 0.396 μA/cm^2 due to the ionized oxygen induced from the bombardment of electrons on the crucible. During the IAD, an oxygen flow rate of 6 ml/min was introduced into the discharge chamber of the cold hollow cathode ion gun and the discharge current associated with the ionization of the oxygen was kept as 0.4 A. The latter means that the amount of ionized oxygen or the concentration of activated oxygen could be fixed in the deposition chamber. The energy of the ionized oxygen was determined by the ion beam potential (V_i) of the oxygen gas gun and was changed from 0

to 300 V during the Sn evaporation. The base pressure of the deposition chamber was 6×10^{-6} Torr while the deposition process was conducted at a working pressure of 1.5×10^{-4} Torr and a substrate temperature of less than 70°C.

Based on the measurements of the deposition rate of tin oxide and the ion current density, the ion/atom arrival ratio (R_i) and the average energy of the atom (E_{ave}) were estimated; they are summarized in Table 1 along with the experimental conditions. It was assumed that the Sn beam consists of a single atom and the SnO_2 structure is rutile with octahedral symmetry ($a = 4.737$ Å, $c = 3.185$ Å, 6 atoms/unit cell if SnO_2).

Two methods for the deposition of the three pairs of IDT (interdigital transducer)-shaped Pt electrodes onto the films were used using a mask and ion sputtering method as shown in Fig. 1. As one case, the deposition of the Pt electrodes was conducted before that of tin oxide thin films while, in the second case, the deposition of the Pt electrode was conducted after that of the thin films. The Pt electrode was 0.5 mm wide, with 0.5 mm spacing and 600 Å thickness, as shown in Fig. 1. An ultrathin (up to 6 Å) noble metal film such as Pt or Pd was then sputter-deposited as an activator layer onto the top of the tin oxide thin film layer. As-fabricated SnO_{2-x} thin film sensors were then heated at 500°C for 1 h using a screen printed Pd-Ag paste heater in air atmosphere. The schematic cross section of a thin film type SnO_{2-x} gas sensor is shown in Fig. 1.

2.2 *Thin film characterization*

The material properties of the synthesized thin films such as structure and composition were determined by XRD (Phillips PW7602), XPS (Surface Science Instruments 2803-S

Table 1
The experimental conditions of tin oxide thin films deposited by IAD, and calculated ion/atom arrival ratios and average energy/atom,

Ion beam potential (V) V_I	Ion current density (μA/cm^2) J_t	Ions/atom arrival ratio R_i	Energy/atom (eV/atom) E_{ave}
0	1.698	0.0467	–
300	16.980	0.4213	123.44
500	27.593	0.6846	337.40
1000	55.185	1.6377	1626.00

Formulas used for calculation.

Ion current density of Neutral-MB without gas ion gun: $J_{N\text{-}MB} = 0.3962$ μA/cm^2

$J_G = J_t - J_{N\text{-}MB}$

$n = R \times 10^{16} / [71.5/\{(1 + (2 - x)) \times 2\}]$

$R_i = 6.25 \times 10^{18} \times J_t/n$

$E_{ave} = V_I \times 6.25 \times 10^{18} \times J_G/n$

assumed octahedral symmetry structure,

$a = 4.737$, $c = 3.185$ Å, 6 atom/cell in structure → Volume 71.5 Å

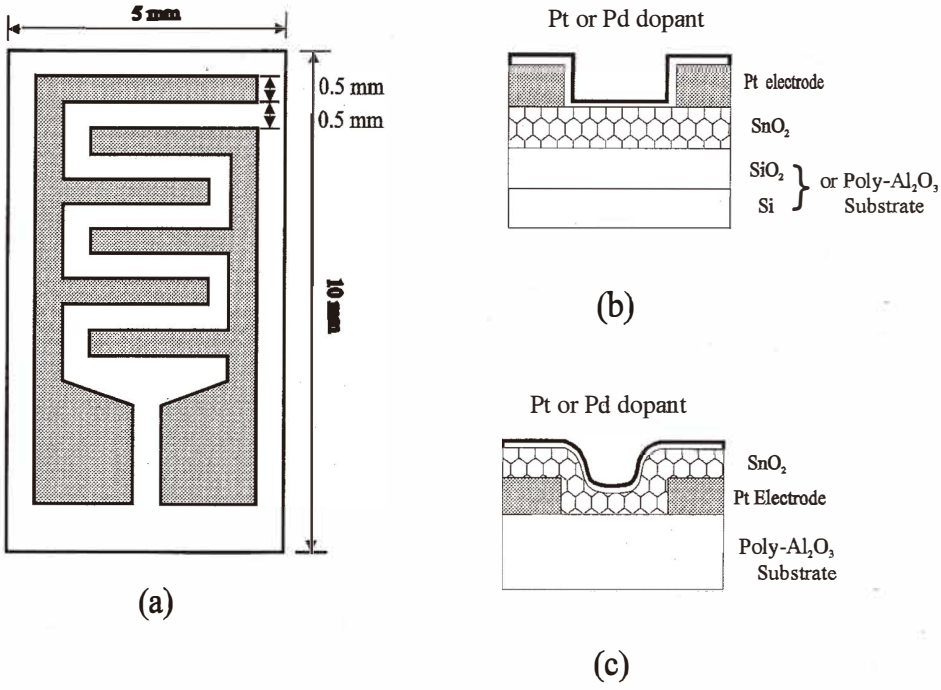

Fig. 1. Schematic structure of a SnO_2 thin film sensor element.

spectrometer), AFM (Park Science Instrument) and TEM (JEOL JEM-2000EX, 200 kV). XRD measurements (30 mA, 40 kV) were conducted to investigate the crystalline structure of as-deposited and annealed tin oxide film prior to the deposition of the Pt electrodes and activator layers. XPS (Al k_a X-ray 1486.6 eV) was carried out to determine the composition ratios and chemical state of the films using adventitious carbon 1*s* transition intentionally allowed as a reference. The surface morphology including surface roughness of the prepared tin oxide films was investigated by AFM and their mictrostrucrures were examined using TEM.

2.3 *Hydrocarbon gas detection*

Gas detection of the synthesized SnO_2 thin film sensors was made for hydrocarbon gases (methane and propane) as functions of temperature and gas concentration. The sensitivities and response times under various conditions were determined in terms of the output voltage of a load resistor (5 kΩ) recorded at an interval of 0.33 s using an Autoranging Microvolt DMM (Keithley 197A) interfaced with a personal computer. The resistor was connected in series to the sensor devices at an input voltage of 9 V. The gas sensitivity (s) was estimated by

$$s(\%) = \frac{(R_{air} - R_{gas})}{R_{air}} \times 100$$

where R_{air} is the resistance in air. The concentration of methane and propane for the tests was fixed at 3000 ppm.

3. Results and Discussion

3.1 *Formation of the SnO_{2-x} thin films (structure and composition)*

Figure 2 shows the X-ray diffraction patterns of the as-deposited and annealed SnO_{2-x} thin film at ion beam voltages of 0 and 300 V. Before annealing, the as-deposited SnO_{2-x} thin film showed an amorphous state with no distinguishable diffraction peak. However, thermal treatment at 500°C for 1 h led to the formation of SnO_2 polycyrstalline structures of <110>, <101> and <211>. In addition, the employment of ion beam potential of 300 V shows the elevated effect of annealing which indicates the formation of the crystalline structure, as observed in Fig. 2. This result indicates that the crystal structure of the

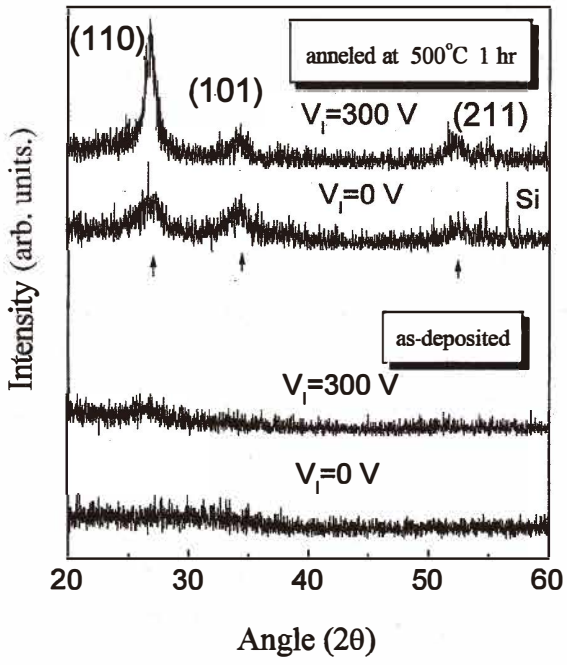

Fig. 2. XRD patterns for the thin oxide thin film deposited by oxygen-ion-assisted deposition under as-deposited and annealed conditions.

deposited film can be controlled using annealing temperature and ion energy. The relative intensity of <110> was observed to be higher as compared to those of <101> and <211>, indicating the existence of some degree of a preferred orientation. It was found from previous studies and works[7,8] that ion beam deposition at low energy yields the preferential crystalline structures of low indices while that at high energy produces those of high indices. Since the process of ion beam deposition is a growth phenomenon at the film surface, the kinetics of the film formation is evidently influenced by the ion energy. Other thermally activated processes, such as the relief of residual stress in the deposited film as well as the transformation to a thermodynamically stable structure, are also affected by the annealing process. In the annealed condition, using Scherrr's formula, the average grain sizes of the deposited film A (0 V) and B (300 V) were determined to be about 8.6 and 17.6 nm, respectively. This result agrees well with the electron diffraction and bright field TEM image observations.

From the electron diffractograms, the amorphous and crystalline features were also confirmed before and after annealing. From the AFM, the surface of the as-deposited film appeared to be very smooth, which is typical in the process of IAD because the mobility of the film surface growth is relatively fast. Figure 3 shows a selection of TEM micrographs of the annealed tin oxide thin film along with transmission electron diffractograms (TED) of selected areas of the films. The rings in the TED patterns are sharp and fairly continuous, showing that the annealed thin films are polycrystalline ones. Another apparent feature is the relative homogeneity at the submicron scale and small grain sizes of less than 10 nm. In the case of semiconducting powder materials, the smaller particle yields higher gas sensitivity due to the relatively increased proportion of the surface space charge layer (electron-depleted zone),[9,10] however, for the thin-film semiconductor, the tin

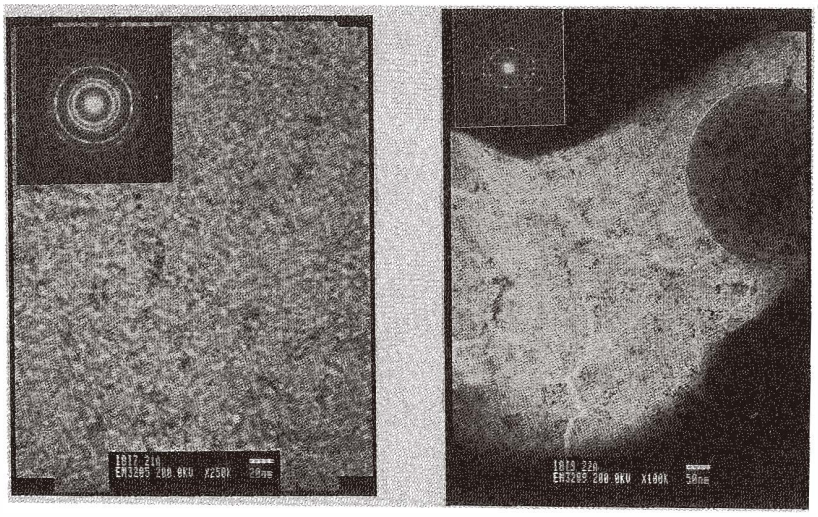

(a) (b)

Fig. 3. TEM micrographs and electron diffractograms of selected areas of the tin oxide thin film deposited by oxygen-ion-assisted deposition under (a) as-deposited and (b) annealed conditions.

oxide thin-film sensor of smaller grain size provides not only highly sensitive (active) sites of gas adsorption on grain boundary but also superior transducer function due to its dense structure. Hence, increased gas sensitivity was expected for smaller grain sizes.

The atomic ratios of the deposited tin oxide thin film were estimated using XPS spectra. Figure 4 shows the Sn3*d* and O1*s* transitions of XPS spectra for as-deposited and annealed SnO_{2-x} thin film. From the XPS analysis of standard stoichiometric SnO_2 powder,[7] the binding energies of Sn3$d_{5/2}$, Sn3$d_{3/2}$, and O1*s* are 486.72, 495.17 and 530.58 eV, respectively, and the full width at half maximum (FWHM) is 1.37, 1.33 and 1.29 eV, respectively. It was found that, although the observed FWHM appeared to be slightly broader (Sn: 1.46 –1.80 eV, O: 1.37–1.54 eV), the binding energies determined from the XPS spectra coincided with those of the standard one. Also, the binding energy separation (O1*s* – Sn3$d_{5/2}$) ranging from 43.78 eV to 43.87 eV with ion energy agreed well with the standard one of 43.88 eV. Hence, the stoichiometry of the synthesized tin oxide films was evaluated to be close to that of $SnO_2(Sn^{4+})$. To gain more accurate atomic ratios of Sn/O, the peak areas of Sn3$d_{5/2}$ and O1*s* were used, taking into consideration the atomic sensitivity factors. In the as-deposited condition, the value of x in SnO_{2-x} was found to be 0.29, indicating oxygen deficiency; after thermal treatment, a slight oxygen sufficiency (x = 0.02) was observed, implying the occurrence of oxidation in the course of annealing.

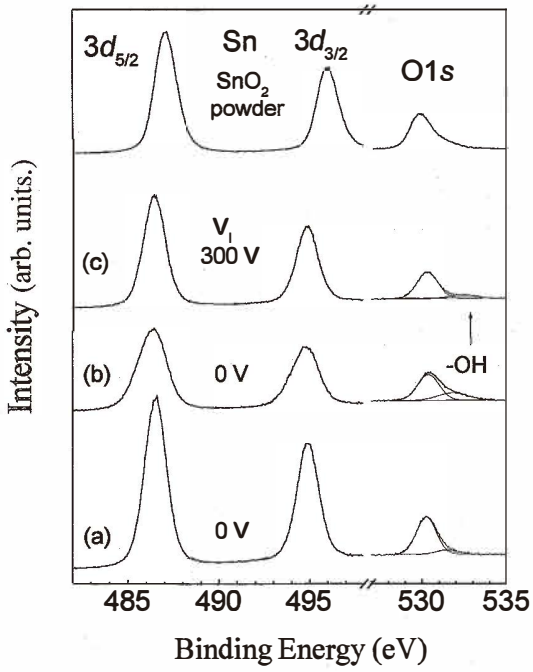

Fig. 4. XPS spectra of as-deposited (a) and annealed tin oxide thin film at 500°C (b,c) at V_i = 0 V (a,b) and 300 V (c).

3.2 *Methane and propane sensitivities*

The layer structure of the thin film sensor employed was Pt(xÅ)/Pt electrode (upper position)/SnO_2(400 Å)/SiO_2/Si substrate (see Fig. 1(b)). The Pt layer of a few Å thickness was applied as a dopant, followed by thermal treatment to provide appropriate active sites for gas adsorption. In general, systematic studies for sensors start from undoped materials and then introduce different bulk or surface intrinsic and extrinsic (foreign atom) dopants to increase gas sensitivity. Therefore, the detection sensitivity of the thin-film sensors was determined with varying Pt dopant layer thickness (amount) of 0, 6, 10, 14 and 18 Å.

Figure 5 shows the variations of gas sensitivity of an undoped SnO_2 thin-film sensor in the temperature range of 100°C to 500°C at CH_4 and C_3H_8 of 3000 ppm and an ion beam energy (V_i) of 0 V. The sensitivity for CH_4 did not change significantly with temperature while the sensitivity for C_3H_8 was increased with temperature up to 45%. At lower temperatures, no distinguishable difference in gas sensitivity was observed between CH_4 and C_3H_8 but, as temperature increased, the sensitivity for C_3H_8 increased. This result can be understood by the fact that the film conductance is affected by ionic point defect (*e.g.* oxygen vacancies V_o) resulting from film nonstoichiometry and hence appropriate heating will increase the rate of oxygen adsorption with receiving electron from the film, and CH_4 is chemically more stable than C_3H_8, implying less sensitivity for CH_4 than that for C_3H_8.

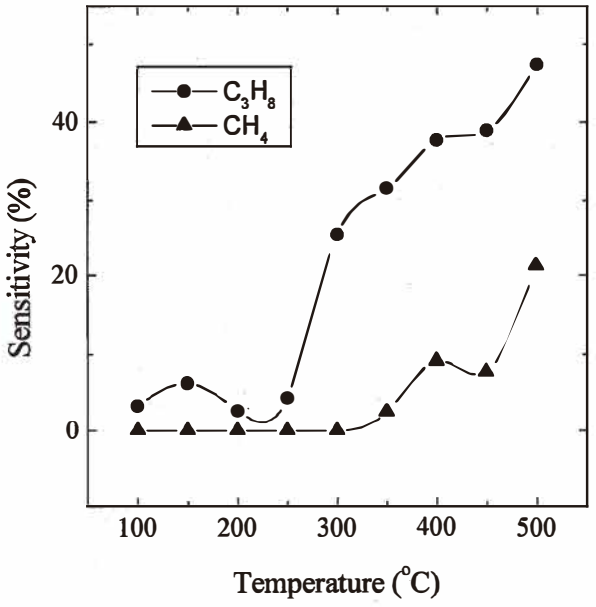

Fig. 5. Variation of detection sensitivity for an undoped SnO_2 thin-film sensor as a function of temperature for methane and propane at 3000 ppm.

However, it appears that the addition of Pt dopants yielded greater sensitivity for CH_4 as compared to that for C_3H_8 at lower temperatures but, at higher temperatures, the sensitivity for C_3H_8 was observed to be higher over that for CH_4 except for the case of Pt (18 Å) doping. Figures 6(a) – 6(d) represent the sensitivity of the thin-film sensor for CH_4 and C_3H_8 of 3000 ppm with temperature, as the thickness of the Pt layer (Pt-doping) was varied from 6 to 18 Å. As compared to Fig. 5, enhancement of the gas sensitivity was generally achieved by Pt doping as expected.[11,12]

For 18-Å-thick Pt doping of the SiO_2/Si substrate, Fig. 6(d) shows the results of the gas detection tests conducted as a function of temperature, using sample gases of 3000 ppm CH_4 and 3000 ppm C_3H_8. In both cases, as the substrate temperature varied, higher sensitivity was observed in the temperature range between 150°C and 450°C. An interesting feature to note is that the sensitivity for CH_4 was observed to be higher as compared to that for C_3H_8 in terms of the fact that, in most cases, the detection of CH_4 is more difficult than that of C_3H_8 or other gases. This means that the tin oxide thin film synthesized by IAD might be optimally used to construct a good gas sensor for the detection of CH_4 in the presence of C_3H_8, based on the employment of sensitivity discrepancy of both gases. However, this phenomenon was not observed when Pt electrode was deposited before the formation of the tin oxide layer (Pt(xÅ)/SnO_2(400 Å)/Pt electrode (lower position)/SiO_2/Si substrate, see Fig. 1(c). As the amount of Pt doping increased further from 18 Å, the relative sensitivity for methane decreased. Therefore, the improved detection sensitivity for methane seemed to depend on the appropriate amount of Pt dopant along with the Pt electrode position. The effect of the electrode position implies that the methane sensing is dominantly related to catalytic gas adsorption and the reaction process on the surface rather than the subsurface and bulk diffusion process through the film. However, the detailed understanding of the gas sensing mechanism needs the consideration of numerous factors along with extensive tests.

Figures 7(a) – 7(c) represent the different effects of Pd dopant but, in this case, the SnO_2 thin film was deposited with an ion energy of 300 V after a series of screening tests. As observed in the Pt doping, the addition of Pd dopant yielded an increase in the sensitivity for CH_4 at lower temperatures. Figure 7(b) (6 Å-Pd /upper Pt electrode position) shows an interesting feature that a higher sensitivity (50%) for CH_4 was determined at a lower temperature of 150°C. This result is thought to be related to the formation of the denser film and increased grain size in E = 300 eV along with the presence of Pd, which yields the relatively higher sensitivity of CH_4 over C_3H_8. This result also indicates a possibility of lowering the optimal detection temperature for CH_4 while maintaining the appropriate gas sensitivity. However, such an observation (high sensitivity at low temperatures) was not made in the case of different amounts of Pd doping (3, 12 Å).

With regard to propane detection, an alumina plate rather than an SiO_2/Si plate was chosen as a substrate, since alumina substrates produced better sensitivity from screening tests. In the case of propane detection, the lower electrode position was observed to be more effective, which indicates the influence of subsurface and bulk diffusion through the films. Hence, in this case, the Pt electrode was deposited before the deposition of the tin oxide layer (lower electrode position). As shown in Fig. 8, a higher sensitivity (71.4%, 3.5 times) for C_3H_8 at 400°C was determined using a 6-Å-Pt-doped SnO_2 thin film (1300 Å)

(a)

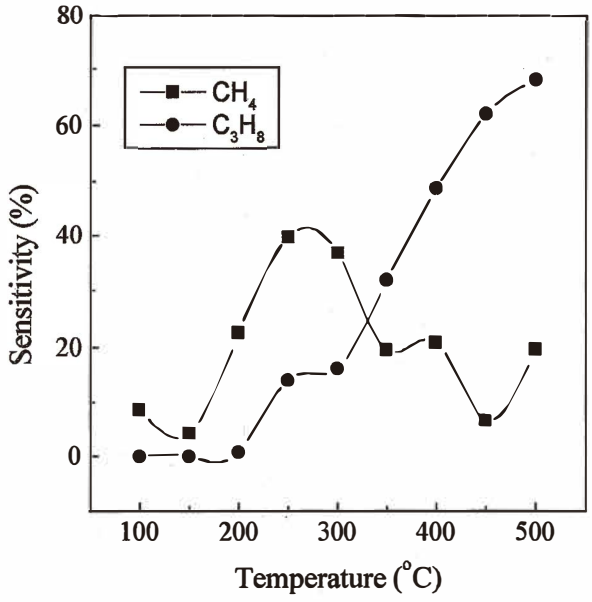

(b)

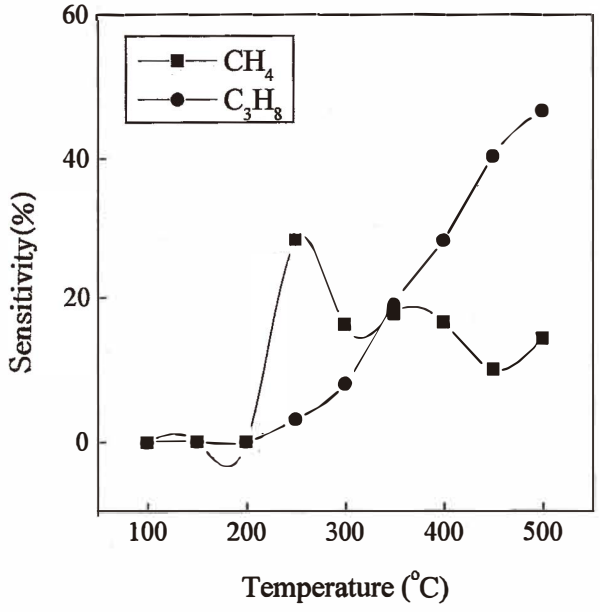

Fig. 6. Variation in detection sensitivity of Pt-doped SnO_2 thin-film sensors as a function of temperature for methane and propane at 3000 ppm. (a) Pt 6 Å (b) Pt 10 Å.

(c)

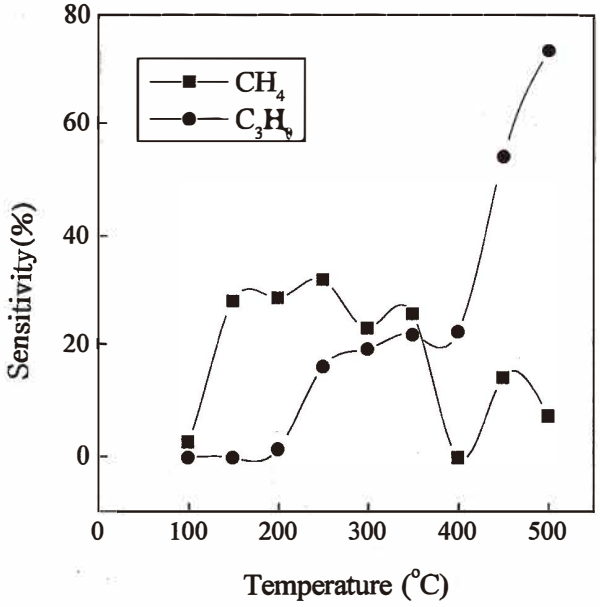

(d)

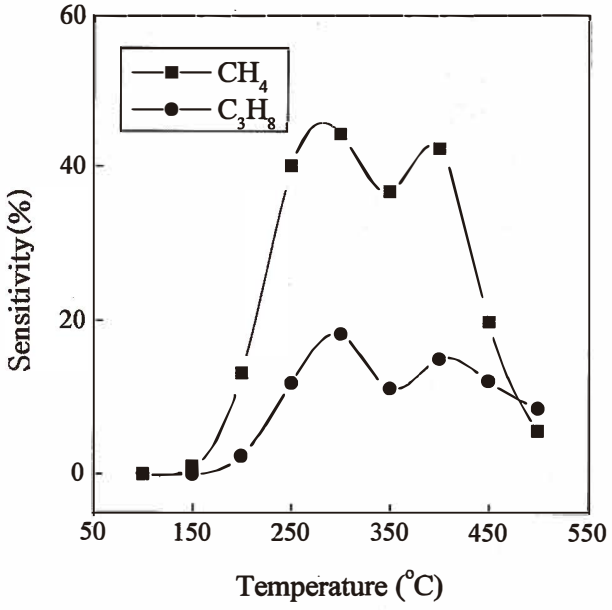

Fig. 6. Variation in detection sensitivity of Pt-doped SnO_2 thin-film sensors as a function of temperature for methane and propane at 3000 ppm. (c) Pt 14 Å (d) Pt 18 Å.

(a)

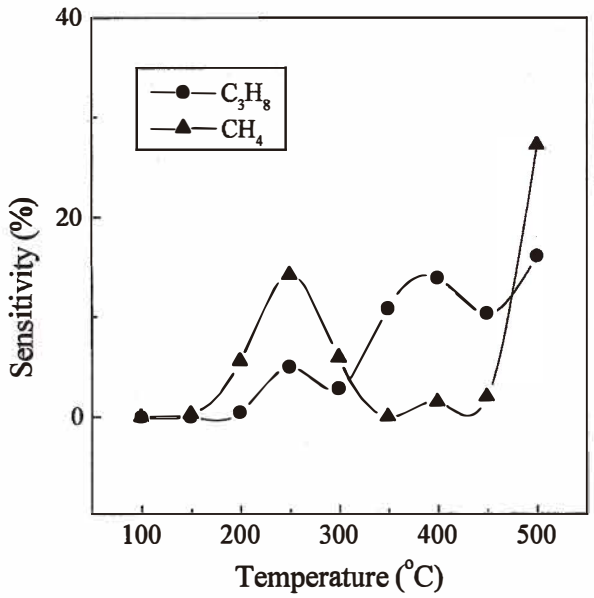

(b)

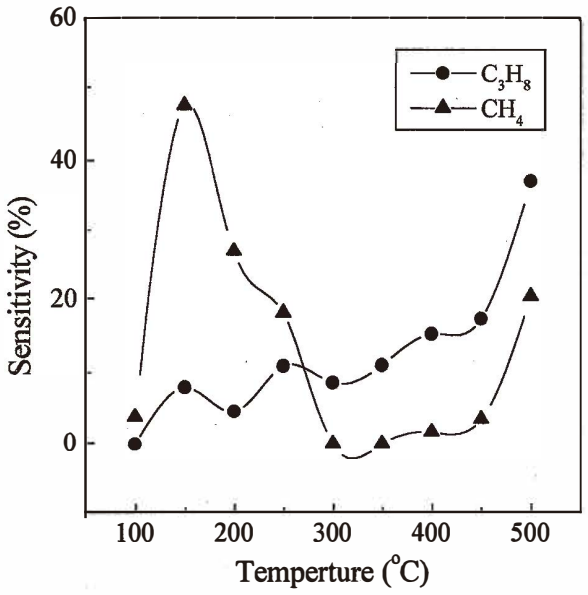

Fig. 7. Variation in detection sensitivity of Pd-doped SnO_2 thin-film sensors as a function of temperature for methane and propane at 3000 ppm. (a) Pd 3 Å (b) Pd 6 Å.

(c)

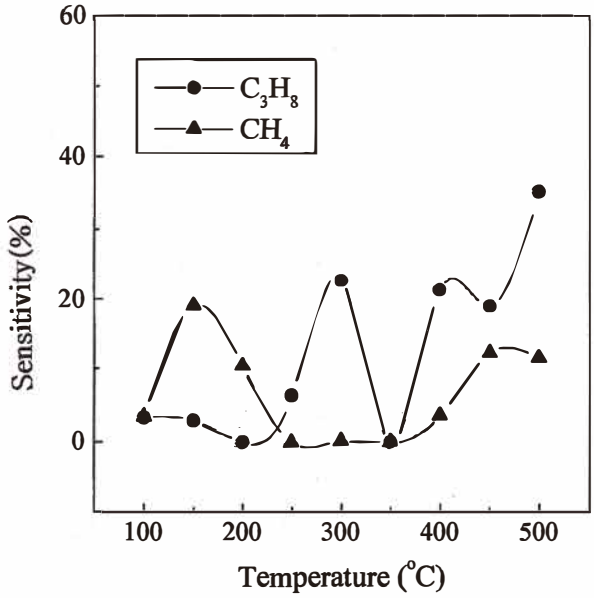

Fig. 7. Variation in detection sensitivity of Pd-doped SnO_2 thin-film sensors as a function of temperature for methane and propane at 3000 ppm. (c) Pd 12 Å.

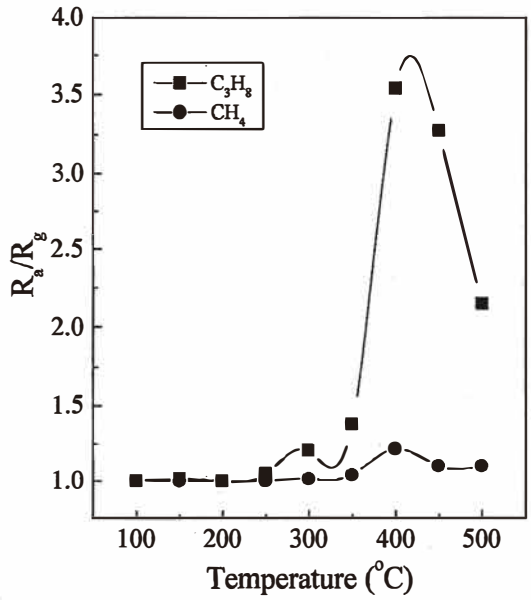

Fig. 8. Variation in resistance with gas (R_g) and without gas (R_a) for a Pt-doped SnO_2 thin-film (1300 Å) sensor as a function of temperature for methane and propane at 3000 ppm.

sensor. Figure 9 shows the results of the sensitivity variation for C_3H_8 with temperature under various conditions. There was a tendency for the propane sensitivity to increase with increasing temperature when the ion beam potential was increased to 300 V and the thickness of the SnO_2 layer was 2000 Å (undoped or doped (6 Å)/SnO_2 layer/Pt electrode/ Al_2O_3 substrate). In addition, the dopant addition was not quite as influential when compared to that for methane detection on Si substrate. However, based on the fact that the detection sensitivity must be greater than 60% for a commercial gas sensor, this type of gas sensor with appropriate amount of Pt dopant and Al_2O_3 substrate might be used effectively in lowering the minimum operating temperature from a typical one of 350 to 250°C. The reduction in the detection temperature seems possible because of the ample surface sites of the alumina substrate (1 μm surface roughness) for gas adsorption and diffusion.

The response and recovery times for propane detection (93.4% sensitivity) are shown in Fig. 10. Based on Pd (6 Å)-doped SnO_2 on alumina substrate with 3000 ppm propane, both the response and the recovery times were 1.8 s at 190°C. However, for the case of methane detection, no distinguishable sensitivity was observed and hence, this sensor element could be suitable for propane detection, since it enables a lower sensing temperature (from above 300°C to under 200°C) with a stable response.

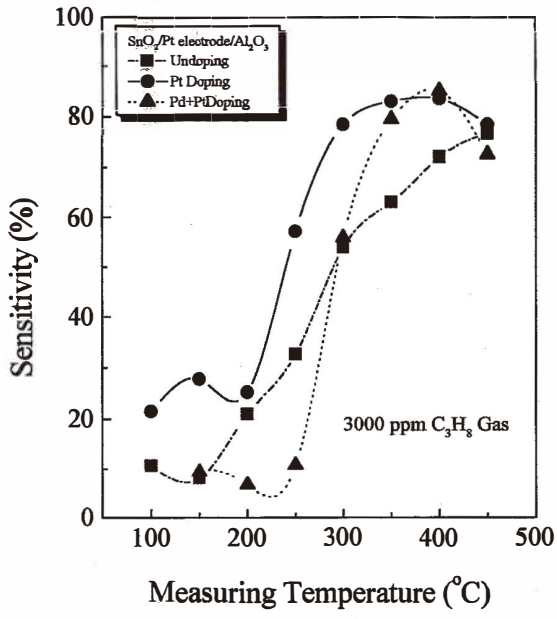

Fig. 9. Variation in sensitivity of a Pt-doped SnO_2 thin film for propane at 3000 ppm at various temperatures.

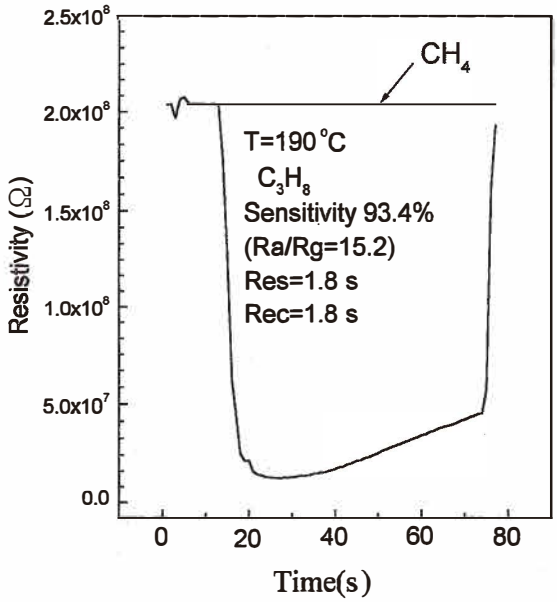

Fig. 10. Response time of a Pd (6 Å)-doped SnO_2 element on an Al_2O_3 substrate.

4. Conclusions

By using oxygen IAD at room temperature with varying ion beam energy, tin oxide thin films were formed on SiO_2/Si and alumina substrates and then tested for hydrocarbon gas (CH_4 and C_3H_8) detection using dopants, operating temperature and electrode position. The as-deposited tin oxide thin films were primarily in an amorphous state and the annealed films showed a preferred orientation along the <110> axis, along with <101> and <211>. All the deposited films showed a deficiency in oxygen content as the state of SnO_{2-x} but had a binding energy of Sn^{+4}.

In the case of methane detection, based on SiO_2/Si substrates, the upper electrode position with Pt doping (18 Å) yielded better sensitivities of methane over propane, implying that the sensing of methane dominantly depends on the surface gas adsorption and reaction. In addition, an increase in ion potential from 0 to 300 V with Pd doping (6 Å) showed a possibility of lowering the operating temperature. On the other hand, in terms of propane detection, a lower electrode position produced improved sensing results, indicating that the sensing of propane is related not only to the surface reaction but also the subsurface and bulk diffusion processes through the films. In this case, using alumina substrates additionally led to improved sensing properties of the elements with decreasing operating temperature.

The tendency of temperature effects on propane sensitivity agrees with the general observation in SnO_2-based gas sensors. However, from the results of methane detection with Pt doping and Si substrate (increased sensitivity at lower temperatures), the sensing mechanism of CH_4, appearing to be dominantly affected by the catalytic adsorption on the surface, is obviously different from that of C_3H_8.

References

1 C. Wagner: J. Chem. Phys. **18** (1950) 69.
2 T. Seiyama, A. Kato, K. Fujiishi and M. Nagatani: Analytical. Chem. **34** (1962) 1502.
3 J. Watson: Sensors and Actuators **5** (1984) 29.
4 Y. Matsuura, K. Takahata and K. Ihokura: Sensors and Actuators **14** (1988) 223.
5 D. Kohl: Sensors and Actuators **18** (1989) 71.
6 P. T. Moseley: Sensors and Actuators B **3** (1991) 167.
7 S. K. Song, W. K. Choi, J. S. Cho, H. J. Jung, D. Choi, J. Y. Lee, H. K. Baik and S. K. Koh: Jpn. J. Appl. Phys. **36** (1997) 2281.
8 S. K. Song, W. K. Choi, J. S. Cho, H. J. Jung, S. K. Koh, D. Choi and H. K. Baik: Submitted to Sensors and Actuators.
9 N. Yamazoe and N. Miura: Some basic aspects of semiconductor gas sensors in Chemical Sensor Technology, vol.4 ed. S. Yamaguchi (Kodansha, Tokyo, 1992) 19.
10 N. Yamazoe: Sensors and Actuators B **5** (1991) 7.
11 W. Gopel, J. Hesse and J. N. Zemel: Sensors, A. Compresensive Survey, Vol. 2, Chemical and Biochemical Sensors, Part I, VCH Weinheim (1991) 119.
12 G. Silz, G. Kuhner, H. Reiter, G. Uptmoor, W. Schweizer, H. Low, M. Lacher and K. Steiner: Sensors and Actuators B **15**–**16** (1993) 390.